Magnetic Control of Potential Microrobotic Drug Delivery Systems: Nanoparticles, Magnetotactic Bacteria and Self-Propelled Microjets

Islam S. M. Khalil*, Veronika Magdanz†, Samuel Sanchez†, Oliver G. Schmidt†‡,
Leon Abelmann*♭ and Sarthak Misra*

*University of Twente, PO Box 217, 7500 AE Enschede, The Netherlands
†Institute for Integrative Nanosciences, IFW Dresden, Helmholtzstr. 20, 01069 Dresden, Germany
‡Material Systems for Nanoelectronics, University of Technology Chemnitz,
Reichenhainer Strasse 70, 09107 Chemnitz, Germany

Abstract— Development of targeted drug delivery systems using magnetic microrobots increases the therapeutic indices of drugs. These systems have to be incorporated with precise motion controllers. We demonstrate closed-loop motion control of microrobots under the influence of controlled magnetic fields. Point-to-point motion control of a cluster of iron oxide nanoparticles (diameter of 250 nm) is achieved by pulling the cluster towards a reference position using magnetic field gradients. Magnetotactic bacterium (MTB) is controlled by orienting the magnetic fields towards a reference position. MTB with membrane length of 5 μm moves towards the reference position using the propulsion force generated by its flagella. Similarly, self-propelled microjet with length of 50 μm is controlled by directing the microjet towards a reference position by external magnetic torque. The microjet moves along the field lines using the thrust force generated by the ejecting oxygen bubbles from one of its ends. Our control system positions the cluster of nanoparticles, an MTB and a microjet at an average velocity of 190 μm/s, 28 μm/s, 90 μm/s and within an average region-of-convergence of 132 μm, 40 μm, 235 μm, respectively.

I. INTRODUCTION

Magnetic microrobots have the potential to deliver concentrated pharmaceutical agents to diseased cells to avoid the negative side-effects associated with chemotherapeutical treatment [1], [2]. Many researchers proposed the utilization of biodegradable magnetic nanoparticles [3], [4], magnetotactic bacteria [5], artificial swimmers [6], and self-propelled microjets [7], [8] to execute limited tasks, such as targeted drug delivery [9], microassembly [10], and microactuation [11]. Realization of a reliable drug targeting system necessitates the development of precise closed-loop motion control systems. Kummer *et al.* developed and utilized a 5 degree-of-freedom magnetic system to puncture a blood vessel of a chorioallantoic membrane of a chicken embryo using a magnetic agent (two cubes with edge length of 800 μm) with permanent magnetization [12]. Magnetic control of a single paramagnetic microparticle in the presence of static
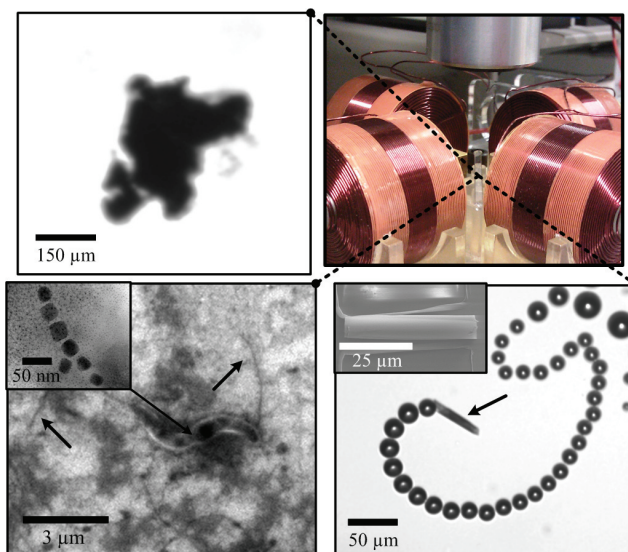

Fig. 1. Magnetic system for the point-to-point motion control of a cluster of iron oxide nanoparticles, magnetotactic bacterium (MTB) and a self-propelled microjet under the influence of the magnetic fields. The upper left image shows a cluster of nanoparticles. Motion of this cluster is achieved by the magnetic field gradients. The bottom left Scanning Electron Microscopy (SEM) image shows the membrane of an MTB (*Magnetospirillum magneticum* AMB-1), and its flagella, indicated by the black arrows. Motion of the MTB is due to the flagella and the external magnetic fields. The inset shows a Transmission Electron Microscopy image of the magnetite nanocrystals enveloped in the membrane of the MTB. The bottom right image shows a microjet moving under the influence of the external magnetic fields and its self-propulsion force. This propulsion force is generated by the ejecting oxygen bubbles from one end of the microjet. The inset shows a SEM image of a microjet fixed to its substrate.

and dynamic obstacles was presented by Khalil *et al.* [13]. Martel *et al.* demonstrated the effectiveness of a swarm of magnetotactic bacteria in the execution of a manipulation task of microobjects under the influence of the controlled magnetic fields [14]. Microassembly of microobjects using a cluster of microparticles (with average diameter of 100 μm) and a magnetic-based manipulation system has been shown by Khalil *et al.* [15]. These magnetic systems can be used for targeted drug delivery by the incorporation of a clinical imaging modality, such as magnetic resonance imaging or ultrasound systems.
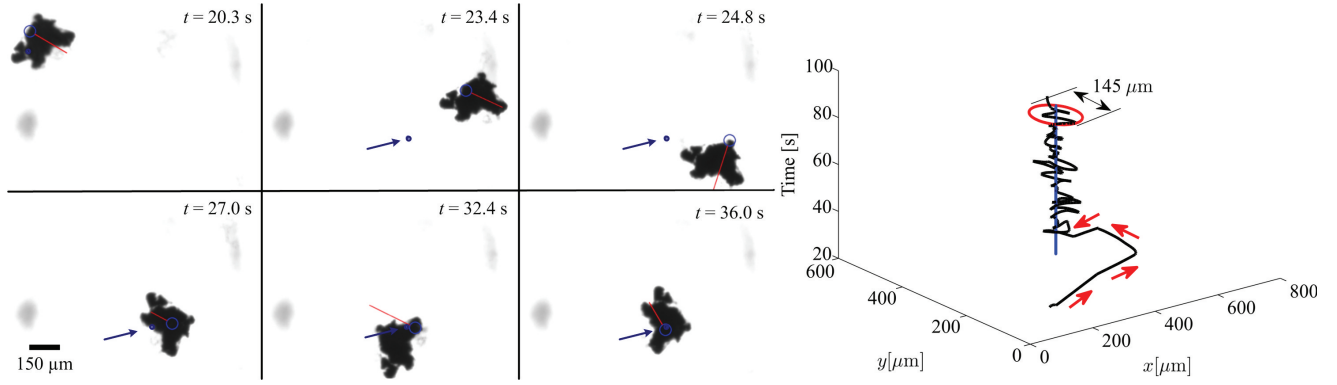
Fig. 2. Closed-loop motion control of a cluster of iron oxide nanoparticles (45-00-252 Micromod Partikeltechnologie GmbH, Rostock-Warnemuende, Germany) under the influence of the controlled magnetic fields. The cluster moves towards the reference position (small blue circle) by the magnetic field gradient generated using control law (8). In this representative experiment, the cluster moves at an average velocity of 195 μm/s, and is positioned by the closed-loop control system within a region-of-convergence of 145 μm in diameter. The entries of each of the diagonal matrices ($\mathbf{K}_\mathrm{p}$ and $\mathbf{K}_\mathrm{d}$) are 0.1 s^{-2} and 0.5 s^{-1}, respectively. The large blue circle is assigned by our feature tracking software [13] and represents the position of the cluster, whereas the red line represents its velocity vector. The blue arrows indicate the reference position. The solid blue line in the right image represents the reference position.

In this work, we present point-to-point motion control of a cluster of iron oxide nanoparticles, magnetotactic bacteria, and self-propelled microjets (Fig. 1) using a closed-loop motion control system. This control system is based on the characterization of the magnetic dipole moment of the aforementioned magnetic objects. Motion control of the nanoparticles is achieved by controlling the gradients of the magnetic fields to pull the nanoparticles towards a reference position, whereas magnetotactic bacteria and microjets are controlled by orienting the fields towards a reference position. Magnetotactic bacteria and microjets move along the magnetic field lines using their self-propulsion forces that are generated by the helical flagella and the ejecting oxygen bubbles, respectively.

II. MODELING AND CONTROL SYSTEM DESIGN

In our work, iron oxide nanoparticles, magnetotactic bacteria and self-propelled microjets move in water, growth medium and hydrogen peroxide solution, respectively. Their motion is also guided using external magnetic fields. Therefore, these magnetic objects experience viscous drag forces and torques, and magnetic forces and torques.

A. Modeling of the Magnetic Objects

Our magnetic objects experience the following magnetic force ($\mathbf{F}(\mathbf{P}) \in \mathbb{R}^{3\times1}$) and magnetic torque ($\mathbf{T}(\mathbf{P}) \in \mathbb{R}^{3\times1}$):

$$\mathbf{F}(\mathbf{P}) = \nabla(\mathbf{m}(\mathbf{P}) \cdot \mathbf{B}(\mathbf{P})) \text{ and } \mathbf{T}(\mathbf{P}) = \mathbf{m}(\mathbf{P}) \times \mathbf{B}(\mathbf{P}), \quad (1)$$

where $\mathbf{m}(\mathbf{P}) \in \mathbb{R}^{3\times1}$ and $\mathbf{B}(\mathbf{P}) \in \mathbb{R}^{3\times1}$ are the induced magnetic dipole moment of the magnetic objects and the magnetic field at point ($\mathbf{P} \in \mathbb{R}^{3\times1}$), respectively. The magnetic dipole moment of the cluster of nanoparticles allows it to align along the external field lines. The nanocrystal chain enveloped in the membrane of the magnetotactic bacteria provides a magnetic dipole moment which allows them to align along the field lines. Similarly, our self-propelled microjets have tubular structure with layers of platinum, titanium and iron [16]. These layers provide a magnetic

dipole moment which allows the microjets to orient along the external magnetic field lines. The cluster of nanoparticles experiences the following drag force ($\mathbf{F}_\mathrm{dc}(\dot{\mathbf{P}}) \in \mathbb{R}^{3\times1}$) and drag torque ($\mathbf{T}_\mathrm{dc}(\boldsymbol{\Omega})$):

$$\mathbf{F}_\mathrm{dc}(\dot{\mathbf{P}}) = F_\mathrm{cl}\eta\dot{\mathbf{P}} \text{ and } \mathbf{T}_\mathrm{dc}(\boldsymbol{\Omega}) = F_\mathrm{cr}\eta\boldsymbol{\Omega}. \quad (2)$$

In (2), F_cl and F_cr are the linear and rotational shape factors of the cluster, respectively. Further, $\dot{\mathbf{P}}$, $\boldsymbol{\Omega}$ and η are the linear and angular velocity of the cluster, and the dynamic viscosity of the fluid (water), respectively. Magnetotactic bacteria and self-propelled microjets also experience the following drag force ($\mathbf{F}_\mathrm{d}(\dot{\mathbf{P}})$) and drag torque ($\mathbf{T}_\mathrm{d}(\boldsymbol{\Omega})$):

$$\mathbf{F}_\mathrm{d}(\dot{\mathbf{P}}) = \gamma\dot{\mathbf{P}} \text{ and } \mathbf{T}_\mathrm{d}(\boldsymbol{\Omega}) = \alpha\boldsymbol{\Omega}, \quad (3)$$

where γ is the linear drag coefficient and is given by [17]

$$\gamma = 2\pi\eta l \left[\ln\left(\frac{2l}{d}\right) - 0.5\right]^{-1}, \quad (4)$$

where l and d are the length and diameter of the MTB and microjet, respectively. In (3), α is the rotational drag coefficient and is given by [18]

$$\alpha = \frac{\pi\eta l^3}{3}\left[\ln\left(\frac{l}{d}\right) + 0.92\left(\frac{d}{l}\right) - 0.662\right]^{-1}. \quad (5)$$

We assume that the microjet has a cylindrical morphology, and its linear and rotational drag coefficients can be modeled using (4) and (5), respectively. A magnetotactic bacterium (MTB) and a microjet also experience self-propulsion forces. These forces are generated by the rotation of the helical flagella [19], and the ejecting oxygen bubbles due to the catalytic decomposition of the hydrogen peroxide solution by the platinum layer of the microjet [8], [16]. Our magnetic system [13] is used to generate controlled magnetic fields to realize the point-to-point motion control.
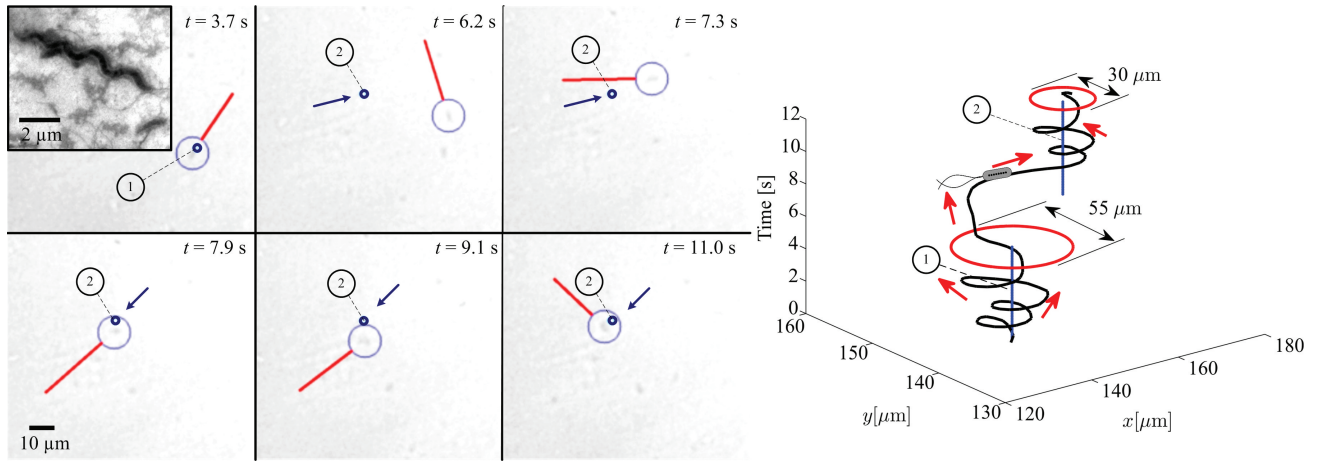
Fig. 3. Closed-loop motion control of a magnetotactic bacterium (MTB), strain *Magnetospirillum magneticum* AMB-1, under the influence of the controlled magnetic fields. An MTB moves towards the reference positions (small blue circles) along the magnetic field lines generated using the control law (8). MTB moves using its helical flagella. In this representative experiment, an MTB moves at an average velocity of 19 μm/s, and is positioned within the vicinity of two reference positions (represented by the solid blue lines in the right image). The closed-loop control system achieves a region-of-convergence of 55 μm and 30 μm in diameter for the first and second reference positions, respectively. The entries of the diagonal matrices ($\mathbf{K}_{\mathrm{p}}$ and $\mathbf{K}_{\mathrm{d}}$) are 15 s^{-2} and 15.5 s^{-1}, respectively. The large blue circle is assigned by our feature tracking software [13] and represents the position of the MTB, whereas the red line represents its velocity vector. The inset shows a Scanning Electron Microscopy image of the spiral membrane of the MTB.

B. Control System Design

Our magnetic system consists of n-electromagnets. The magnetic field $(\mathbf{B}_i(\mathbf{P}))$ is linearly proportional to the applied current (I_i) at the ith electromagnet. Therefore, the magnetic fields at point $(\mathbf{P})$ is given by [12]

$$\mathbf{B}(\mathbf{P}) = \sum_{i=1}^{n} \mathbf{B}_i(\mathbf{P}) = \sum_{i=1}^{n} \widetilde{\mathbf{B}}_i(\mathbf{P})I_i = \widetilde{\mathbf{B}}(\mathbf{P})\mathbf{I}, \quad (6)$$

where $\widetilde{\mathbf{B}}(\mathbf{P}) \in \mathbb{R}^{3 \times n}$ is a matrix which depends on the position at which the magnetic field is evaluated, and $\mathbf{I} \in \mathbb{R}^{n \times 1}$ is a vector of the applied current. The magnetic field due to each electromagnet is related to the current input by $\widetilde{\mathbf{B}}_i(\mathbf{P})$. Substituting (6) in the magnetic force equation (1) yields the following magnetic force-current map:

$$\mathbf{F}(\mathbf{P}) = (\mathbf{m}(\mathbf{P}) \cdot \nabla)\widetilde{\mathbf{B}}(\mathbf{P})\mathbf{I} = \mathbf{\Lambda}(\mathbf{m}, \mathbf{P})\mathbf{I}, \quad (7)$$

In (7), $\mathbf{\Lambda}(\mathbf{m}, \mathbf{P}) \in \mathbb{R}^{3 \times n}$ is the actuation matrix which maps the input current to the magnetic force [12]. Further, we devise the following proportional-derivative control law [15]

$$\mathbf{F}_{\mathrm{des}}(\mathbf{P}) = \mathbf{K}_{\mathrm{p}}\mathbf{e} + \mathbf{K}_{\mathrm{d}}\dot{\mathbf{e}}. \quad (8)$$

where $\mathbf{F}_{\mathrm{des}}(\mathbf{P})$ is the controlled magnetic force which can be realized using (7) through the pseudoinverse of the actuation matrix, and by setting $\mathbf{F}_{\mathrm{des}}(\mathbf{P}) = \mathbf{F}(\mathbf{P})$. Further, $\mathbf{e}$ and $\dot{\mathbf{e}}$ are the position and velocity tracking errors, respectively, and are given by

$$\mathbf{e} = \mathbf{P}_{\mathrm{ref}} - \mathbf{P} \quad \text{and} \quad \dot{\mathbf{e}} = \dot{\mathbf{P}}_{\mathrm{ref}} - \dot{\mathbf{P}}, \quad (9)$$

where $\mathbf{P}_{\mathrm{ref}}$ and $\dot{\mathbf{P}}_{\mathrm{ref}}$ are the reference position and velocity, respectively. Finally, in (8), $\mathbf{K}_{\mathrm{p}}$ and $\mathbf{K}_{\mathrm{d}}$ are diagonal positive-definite gain matrices. In order to implement the control law (8), the pseudoinverse of the actuation matrix $(\mathbf{\Lambda}(\mathbf{m}, \mathbf{P}))$ is calculated based on the magnetic dipole moment and position of the magnetic object [19].

III. EXPERIMENTAL RESULTS

Motion control experiments are done using a magnetic system, shown in Fig. 1. This system consists of four orthogonally oriented air-core electromagnets (n=4). These electromagnets can surround a reservoir, a capillary tube and a petri dish to incubate water, growth media and hydrogen peroxide solution for the cluster of nanoparticles, MTB and microjets, respectively. Our closed-loop control system allows for the positioning of the magnetic objects within the vicinity of a reference position. Fig. 2 shows a representative closed-loop motion control result of the cluster. We observe that the cluster is positioned at an average velocity of 195 μm/s and within a region-of-convergence (ROC) of 145 μm. Magnetotactic bacteria (strain *Magnetospirillum magneticum* AMB-1) are controlled inside a capillary tube with inner thickness and width of 0.2 mm and 2 mm, respectively. Our closed-loop control system positions an MTB at an average velocity of 19 μm/s and within a ROC of 55 μm and 30 μm for the first and second reference positions, respectively (Fig. 3). Control of the microjet is done using 1 ml of hydrogen peroxide solution and Triton X at concentrations of 5% and 5%, respectively. Our control system positions the microjet at an average velocity of 62 μm/s and within a ROC of 150 μm and 140 μm for the first and second reference positions, respectively (Fig. 4). All experiments are repeated 10 times, and we observe consistent results.

IV. CONCLUSIONS AND FUTURE WORK

Point-to-point motion control of magnetic objects is demonstrated using a magnetic-based proportional-derivative control system. A cluster of iron oxide nanoparticles is positioned within the vicinity of a reference position (average ROC is 132 μm) at an average velocity of 190 μm/s ($\sim$2 body length per second) under the influence of the controlled
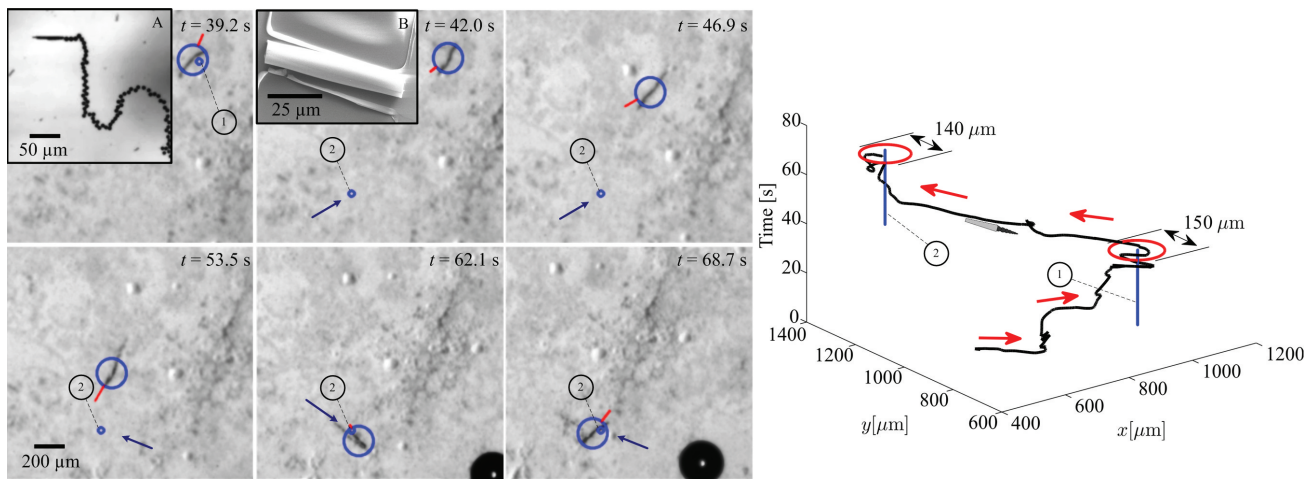
Fig. 4. Closed-loop motion control of a self-propelled microjet under the influence of the controlled magnetic fields. The microjet moves towards the reference positions (small blue circles) along the magnetic field lines generated using the control law (8). The microjet moves along the field lines using the propulsion force generated by the ejecting oxygen bubbles from its end. In this representative experiment, the microjet moves at an average velocity of 62 μm/s, and is positioned within the vicinity of two reference positions (represented by the solid blue lines in the right image). The closed-loop control system achieves a region-of-convergence of 150 μm and 140 μm in diameter for the first and second reference positions, respectively. The entries of the diagonal matrices ($\mathbf{K}_\mathrm{p}$ and $\mathbf{K}_\mathrm{d}$) are 15 s^{-2} and 5 s^{-1}, respectively. This experiment is done using 1 ml of hydrogen peroxide solution and Triton X at concentrations of 5% and 5%, respectively. The catalytic reaction is observed after the addition of 100 μl of hydrogen peroxide solution at concentration of 15%. Inset A shows the ejecting oxygen bubbles from one end of the microjet. Inset B shows a Scanning Electron Microscopy image of a microjet fixed to its substrate. The large blue circle is assigned by our feature tracking software [13] and represents the position of the microjet, whereas the red line represents its velocity vector.

magnetic field gradients. Self-propelled MTB and microjets are controlled at an average velocity of 28 μm/s and 90 μm/s ($\sim$5 and $\sim$2 body length per second), and positioned within an average ROC of 40 μm and 235 μm, respectively.

As part of future work, our magnetic system will be integrated with an ultrasound-based imaging modality. In addition, our magnetic system will be redesigned to control magnetic objects in the three-dimensional space.

REFERENCES

[1] J. Wang and W. Gao, "Nano/microscale motors: biomedical opportunities and challenges," *ACS Nano*, vol. 6, no. 7, pp. 5745-5751, July 2012.

[2] B. J. Nelson, I. K. Kaliakatsos, and J. J. Abbott, "Microrobots for minimally invasive medicine," *Annual Review of Biomedical Engineering*, vol. 12, pp. 55-85, April 2010.

[3] R. Sinha, G. J. Kim, S. Nie, and D. M. Shin, "Nanotechnology in cancer therapeutics: bioconjugated nanoparticles for drug delivery," *Molecular Cancer Therapeutics*, Vol. 5, no. 8, pp. 1909-1917, August 2006.

[4] A. S. Lubbe, C. Bergemann, J. Brock, and D. G. McClure, "Physiological aspects in magnetic drug-targeting," *Journal of Magnetism and Magnetic Materials*, Vol. 194, no. 1-3, pp. 149-155, April 1999.

[5] S. Martel, M. Mohammadi, O. Felfoul, Z. Lu, and P. Pouponneau, "Flagellated magnetotactic bacteria as controlled MRI-trackable propulsion and steering systems for medical nanorobots operating in the human microvasculature," *International Journal of Robotics Research*, vol. 28, no. 4, pp. 571-582, April 2009.

[6] R. Dreyfus, J. Baudry, M. L. Roper, M. Fermigier, H. A. Stone, and J. Bibette, "Microscopic artificial swimmers," *Nature*, vol. 437, no. 6, pp. 862-865, October 2005.

[7] Y. F. Mei, G. Huang, A. A. Solovev, E. B. Urena, I. Monch, F. Ding, T. Reindl, R. K. Y. Fu, P. K. Chu, and O. G. Schmidt, "Versatile approach for integrative and functionalized tubes by strain engineering of nanomembranes on polymers," *Advanced Materials*, vol. 20, no. 21, pp. 4085-4090, November 2008.

[8] A. A. Solovev, Y. F. Mei, E. B. Urena, G. Huang, and O. G. Schmidt, "Catalytic microtubular jet engines self-propelled by accumulated gas bubbles," *Small*, vol. 5, no. 14, pp. 1688-1692, July 2009.

[9] Q. A. Pankhurst, J. Connolly, S. K. Jones, and J. Dobson, "Applications of magnetic nanoparticles in biomedicine," *Journal of Physics*, Vol. 36, no. 13, pp.167-181, July 2003.

[10] S. Martel, "Controlled bacterial micro-actuation," in *Proceedings of the International Conference on Microtechnologies in Medicine and Biology*, pp. 89-92, Okinawa, Japan, May 2006.

[11] S. Sanchez, A. A. Solovev, S. Schulze, and O. G. Schmidt, "Controlled manipulation of multiple cells using catalytic microbots," *Chemical Communication*, vol. 47, pp. 698-700, November 2010.

[12] M. P. Kummer, J. J. Abbott, B. E. Kartochvil, R. Borer, A. Sengul, and B. J. Nelson, "OctoMag: an electromagnetic system for 5-DOF wireless micromanipulation," *IEEE Transactions on Robotics*, vol. 26, no. 6, pp. 1006-1017, December 2010.

[13] I. S. M. Khalil, J. D. Keuning, L. Abelmann, and S. Misra, "Wireless magnetic-based control of paramagnetic microparticles," in *Proceedings of the IEEE RAS/EMBS International Conference on Biomedical Robotics and Biomechatronics (BioRob)*, pp. 460-466, Rome, Italy, June 2012.

[14] S. Martel and M. Mohammadi, "Using a swarm of self-propelled natural microrobots in the form of flagellated bacteria to perform complex micro-assembly tasks," in *Proceedings of the IEEE International Conference on Robotics and Automation (ICRA)*, pp. 500-505, Alaska, USA, May 2010.

[15] I. S. M. Khalil, F. van den Brink, O. S. Sukas, and S. Misra, "Microassembly using a cluster of paramagnetic microparticles," in *Proceedings of the IEEE International Conference on Robotics and Automation (ICRA)*, Karlsruhe, Germany, May 2013. *In Press*

[16] Y. F. Mei, A. A. Solovev, S. Sanchez, and O. G. Schmidt, "Rolled-up nanotech on polymers: from basic perception to self-propelled catalytic microengines," *Chemical Society Review*, vol. 40, no. 5, pp. 2109-2119, May 2011.

[17] H. C. Berg, "Random walks in biology," *Princeton University Press*, Princeton, New Jersey, 1993.

[18] Y. R. Chemla, H. L. Grossman, T. S. Lee, J. Clarke, M. Adamkiewicz, and B. B. Buchanan, "A new study of bacterial motion: superconducting quantum interference device microscopy of magnetotactic bacteria," *Biophysical Journal*, vol. 76, pp. 3323-3330, June 1999.

[19] I. S. M. Khalil, M. P. Pichel, L. Zondervan, L. Abelmann, and S. Misra, "Characterization and control of biological microrobots," in *Experimental Robotics: The 13th International Symposium on Experimental Robotics*, Springer Tracts in Advanced Robotics (STAR), vol. 88, pp. 617-631, 2013.